Nano Energy 58 (2019) 612–623

Contents lists available at ScienceDirect

Nano Energy

journal homepage: www.elsevier.com/locate/nanoen

Full paper

Self-powered multifunctional monitoring system using hybrid integrated triboelectric nanogenerators and piezoelectric microsensors

Changhe Sun[a,b,c,d,1], Qiongfeng Shi[b,c,e,1], Dihan Hasan[b,c,e], Mahmut Sami Yazici[b,c,e], Minglu Zhu[b,c,e], Yiming Ma[b,c,e], Bowei Dong[b,c,e], Yufei Liu[a,d,*], Chengkuo Lee[b,c,e,**]

[a] Centre for Intelligent Sensing Technology, College of Optoelectronic Engineering, Chongqing University, Chongqing 400044, China
[b] Department of Electrical and Computer Engineering, National University of Singapore, 4 Engineering Drive 3, Singapore 117583, Singapore
[c] Center for Intelligent Sensors and MEMS, National University of Singapore, E6 #05-11 F, 5 Engineering Drive 1, Singapore 117608, Singapore
[d] Key Laboratory of Optoelectronic Technology & Systems (Chongqing University), Ministry of Education, Chongqing 400044, China
[e] Hybrid Integrated Flexible Electronic Systems (HiFES), National University of Singapore, Block E6, #E6-5-4, 5 Engineering Drive 1, Singapore 117608, Singapore

ARTICLE INFO

Keywords:
Self-powered
Triboelectric nanogenerator (TENG)
Piezoelectric micromachined ultrasonic transducer (pMUT)
Carbon dioxide (CO_2)
Humidity sensor

ABSTRACT

Battery-less internet of things (IoT) devices and flexible electronics are attracting increasing attention worldwide for diverse applications ranging from human healthcare to environment monitoring. A flexible multifunctional monitoring system with the integration of triboelectric nanogenerator (TENG) for energy harvesting, piezoelectric micromachined ultrasonic transducer (pMUT) array and TENG sensor for simultaneous detection of multiple amenity parameters (i.e., temperature, relative humidity and CO_2 concentration) has been developed. With modification of polyethyleneimine (PEI) on the friction surface, the CO_2 concentration can be sensed by the electrical output of the TENG sensor in a wide range up to 12,000 ppm. To precisely calibrate the effect of humidity on the TENG sensor, pMUT array is integrated that can be potentially powered by another unmodified TENG through harvesting ambient mechanical energy. The pMUT array is coated partially with PEI/graphene oxide (GO) composite and adopted to simultaneously detect relative humidity using functionalized pMUT elements and room temperature using unfunctionalized elements. After optimization of PEI volume fraction in the composite, the pMUT humidity sensor exhibits an extremely high sensitivity (748 Hz/% RH) and relative sensitivity (290 ppm/% RH), an excellent linearity over a wide range, rapid response/recovery, small hysteresis, good stability and significant selectivity over CO_2 gas. Additionally, the pMUT temperature sensor shows an excellent linear response, which is much advantageous to eliminate the temperature interference of the humidity sensor due to the shared array structure. This work demonstrates not only a new and effective route of ultrasensitive and linear humidity detection, but also a new strategy to configure an "all-in-one" flexible self-powered multifunctional sensing system, which complementally combines the advantages of TENG and micro-electro-mechanical-system (MEMS) technology enabled devices and is highly promising to facilitate various applications.

1. Introduction

Over the last decade, internet of things (IoT) as a global dynamic information network closely linking any objects and people on internet, has experienced tremendous growth and reached every corner of this world. The IoT has brought us a promising way to develop portable, miniaturized and multifunctional systems by integrating vast types of sensors for healthcare, biomedical detection, environmental monitoring, remote controls, and security [1–3]. Meanwhile, more and more wearable electronics including diversified wearable sensors have been developed rapidly over the last decade as well, to enable direct and real-time healthcare monitoring from human body [4–8]. Recently, various types of wearable sensors attached on human skin have been demonstrated for the applications ranging from the detection of body motion to the monitoring of physiological parameters, e.g., pressure [9,10], strain [11], temperature [12], and perspiration [13], etc. These

* Corresponding author at: Centre for Intelligent Sensing Technology, College of Optoelectronic Engineering, Chongqing University, Chongqing 400044, China.
** Corresponding author at: Department of Electrical and Computer Engineering, National University of Singapore, 4 Engineering Drive 3, Singapore 117583, Singapore.
E-mail addresses: yufei.liu@cqu.edu.cn (Y. Liu), elelc@nus.edu.sg (C. Lee).
[1] These authors contributed equally to this work.

https://doi.org/10.1016/j.nanoen.2019.01.096
Received 24 November 2018; Received in revised form 16 January 2019; Accepted 31 January 2019
Available online 01 February 2019
2211-2855/

developed wearable sensors can be further included into the IoT network to perform a more complete monitoring of environment conditions and human healthcare status.

Currently, almost all sensors including various wearable sensors distributed across the IoT network require the power source with small-scale power consumption in microwatt to milliwatt level [14]. The most conventional power supply technology is using the batteries, which may be prohibitively costly and impractical when considering monitoring, recharging, maintaining, replacing and recycling batteries for vastly distributed sensors in billions to trillions [15]. Novel technologies that can harvest energy from the environment or human body can present sustainable self-sufficient power supplies for sensors and micro/nano-systems. Therefore, it is expecting to make the sensors and sensing systems operate independently, sustainably and maintenance-free through adopting the self-powering technology.

The state-of-the-art mechanisms of harvesting the external energy can be mainly classified into pyroelectric [16], photovoltaic [17], electromagnetic [18], piezoelectric [19] and triboelectric effects [20]. Among these technologies, triboelectric nanogenerator (TENG) based on triboelectrification (i.e., contact electrification) and electrostatic induction reported firstly by Z. L. Wang's research team in 2012, has drawn world-wide attention due to its outstanding features of sustainability, tremendous output, unrestricted material selection, and simplistic and flexible structure [21–28]. A typical TENG can generate electricity from any type of mechanical energy including human motions [29–31], water wave [32–34], wind flow [34–37] and vibrations [38–40] with a demonstrated total energy conversion efficiency of up to 85% [41]. Besides, the TENG itself can serve as a self-powered active physical sensor for detecting location, displacement, rotation, amplitude, velocity and acceleration [42–46], or biochemical sensor for detecting various gases, humidity, ion and biomolecules [47–56]. However, the versatile nature of TENG based sensors also indicates such devices have to suffer lots of interference from humidity, temperature and particles, leading to a reduction in the electrostatic charge density and sensing accuracy [49,57,58]. In contrast, these detrimental effects can be easily and precisely calibrated with traditional mechanical resonant sensors [59–63] or electrical impedance sensing methods [64–67]. The Si based microelectromechanical system (MEMS) fabrication technology paves a feasible way to miniaturize traditional sensors, enabling the integration of traditional sensors with TENG on a flexible platform through transferring technology, i.e., an “all-in-one” self-powered multifunctional sensing microsystem.

Indoor amenity monitoring is with great significance in the modern society since people are spending most of the time indoor living, working or even exercising. Indoor amenity monitoring includes three important parameters, that is, CO_2 concentration, humidity and temperature. As a promising energy harvesting technology, TENG has been developed as an effective approach for self-powered CO_2 monitoring through functional layer coating on the friction surface, with great potential for battery-less applications [42]. However, common TENGs are highly susceptible to humidity that can lead to dramatic degradation of performance and thereby high variation in terms of sensing when using the self-generated signals. Thus for TENG based sensors, their outputs should be carefully calibrated according to humidity. Due to the output variation with humidity, on the other hand, TENG without coating can be used as humidity sensor [68]. But the resolution of sensitivity cannot be as high or precise as the MEMS sensors, especially in low humidity range. Thus precise humidity measurement is of great importance in not only triboelectric based monitoring, but also a wide range of applications such as environmental monitoring, industrial process control, agricultural production storage, and medical treatments. Various types of MEMS sensors demonstrate the capability for precise detection of humidity and numerous studies have been devoted for the development of highly sensitive and stable microfabricated humidity sensors [59–63]. Compared with other resonant MEMS sensors [59–62], capacitive micromachined ultrasonic transducer (cMUT) has been proven to be an ultrasensitive approach for mass load detection even at the zeptogram (zg) scale and exhibits an excellent sensing performance towards humidity, owing to low effective mass and quite large active surface [69]. However, such good performance relies highly on a very narrow cavity (~40 nm) and high bias voltage (~50 V), which largely increases the processing difficulty and fabrication cost and limits its application fields. Similar to the array structure and operation mode of cMUTs, piezoelectric micromachined ultrasonic transducers (pMUTs) operating at several volts without specially designed cavity can be easily functionalized with selectively sensitive thin film for humidity sensing. In addition, pMUT itself can also be adopted for temperature sensing.

Till now, various humidity-sensitive materials have been investigated in terms of sensitivity, response, stability, repeatability, hysteresis and linearity [61–63,66,67,70–74], etc. Graphene oxide (GO) has attracted great interest recently because of its layered honeycomb structure, electrical insulation characteristics and abundant hydrophilic oxygen functional groups (carboxyl, hydroxyl and epoxy groups) in each layer [75]. Previous studies have demonstrated high sensitivity, fast response and long term stability of GO functionalized resonators [76,77]. However, pure GO coated resonant sensors suffer poor linearity and large hysteresis in the high relative humidity (RH) level (above 60% RH) attributed to the interlayer expansion stress of GO sheets [76]. Although some compositing technologies have been developed to modify GO material with polymers or metal oxides [72,74,78–80], almost all modifications are found in sensitivity, response and hysteresis except linearity. Polyethyleneimine (PEI) with abundant amine groups has been reported to have good adsorption and desorption of both CO_2 gas and humidity and a high sensing selection over other gas species. On one hand, in views of the chemical bonding between amine groups and hydroxyl groups to suppress the interlayer expansion of GO sheets, the modification of GO with PEI polymer may create an effective route to facilitate both good linearity and high humidity-sensing performance. On the other hand, the PEI polymer can be coated on the contact surface of TENG for CO_2 detection through tracking the change of the surface charge.

Previously, on one hand, flexible wearable electronics based on advanced materials have been developed for the monitoring of CO_2 [81], humidity [82], and temperature [12]. Besides, traditional MEMS sensors can be fabricated on flexible platform using chip-scale transferring technologies [83]. In general, these sensors are normally based on passive mechanisms (e.g., resistive, capacitive etc.) which require external power supply for operation. On the other hand, TENGs have also been reported to be integrated into flexible platforms for various sensing applications, such as the detection of CO_2 [42], C_2H_2 [84], ethanol [85], melamine [86], NH_3 [46], and lactate [44], etc. However, to date, there is no integration of TENGs with traditional MEMS sensors on the same flexible platform for “all-in-one” multi-functionalities. The combination of TENGs and MEMS sensors can provide complementary advantages, e.g., TENGs with energy harvesting capability can act as potential power supply for the MEMS sensors, and then the precise MEMS sensors can provide accurate calibration (such as humidity) to TENG based self-powered sensing.

Herein, in this work, an “all-in-one” self-powered flexible multifunctional monitoring microsystem with a hybrid design by combining TENG and pMUT technologies is developed to realize a comprehensive detection of indoor amenity parameters, i.e., CO_2 gas, relative humidity and temperature. The whole multifunctional sensing microsystem consists of a traditional TENG, a functionalized TENG, and a linear pMUT array with and without some elements coating on flexible platform. Potentially, the energy generated by the traditional TENG from scavenging human motions can be used as power supply for pMUT sensing. The pMUT array was fabricated with the MEMS technology and transferred on the flexible substrate through chip-scale transferring technology. The uncoated pMUT can serve as temperature sensor since its resonance is only affected by the temperature. Once the temperature

is determined, the PEI/GO composite coated pMUT can perform as a linear and precise humidity sensor. Then once the humidity is calibrated by pMUT, the functionalized TENG with PEI coating can function as a self-powered CO_2 sensor. Thus the whole microsystem can realize "all-in-one" self-powered multifunctional monitoring. Optimization of PEI/GO composite films with different PEI volume fractions was performed to target high sensitivity and good linearity. The humidity-sensing and CO_2 sensing mechanisms were also systematically investigated. This work not only demonstrates the capability of pMUT-functionalized humidity sensors in highly sensitive and linear detection, but also unambiguously points out the great potential and significant advantage of integrating macro-fabricated flexible TENG with micro-fabricated sensors for multifunctional applications.

2. Experiment

2.1. Fabrication of multifunctional integrated sensing system

GO aqueous suspension with a monolayer rate of above 98% was prepared by the modified Hummers' method and supplied from Suzhou Tanfeng Graphene Technology Co., Ltd (Suzhou, China). The concentration of original GO suspension is 2 mg/ml. The PEI solution was supplied from Sigma-Aldrich Pte Ltd (Singapore) with concentration of 50% (w/v) in H_2O. In this work, GO suspension and PEI solution were diluted to 1 mg/ml and 0.375% (w/v) by deionized (DI) water, respectively. Then the diluted GO suspension at pH 6 and diluted PEI solution at pH 8 were directly mixed together with a PEI volume fraction of 25%, 50% and 75% (GO: PEI = 3:1, 1:1, 1:3). Compared with the pure GO and PEI solution, the resultant mixture (PEI/GO-0) became flocculent, which was reported previously [87]. Herein, a facile compositing process without the assistance of acid solution was proposed to obtain well-distributed PEI/GO solution, as described in Fig. 1a. After the preparation of PEI/GO-0 mixture, the aqueous solution was mechanically stirred firstly for 10 min using the injection syringe with a 400 μm (in diameter) microneedle to pull and push repetitively, and then sonicated for 20 min. It was demonstrated that the floccule disappeared after such mechanical treatment and the final prepared PEI/GO solution became almost homogeneous but a bit darker due to the amidation reaction between amino groups of PEI and oxygen-containing groups of GO [88].

Fig. 1b shows the schematic illustration of the flexible self-powered multifunctional sensing system, which mainly consists of a linear pMUT array with PEI/GO composite coated elements for humidity detection and uncoated elements for simultaneous temperature detection, a traditional TENG as the potential self-sufficient power supply for pMUTs, a PEI film coated TENG as the active CO_2 sensor, an energy storage circuit (composed of a rectifier, a resistance and a capacitor) and a flexible polyethylene terephthalate (PET) substrate. The generated energy from the traditional TENG is connected to a rectifier circuit and stored in a capacitor as a potential power supply, and at this stage, the pMUT sensors are still powered by external power supply. The linear pMUT array consists of 15 rectangular pMUT elements, some of which are coated with the PEI/GO composite film as relative humidity sensors, while the others are uncoated as reference temperature sensors. The structural configuration of the pMUT array is shown in Fig. 1c, which contains 10 μm Si /1 μm SiO_2/200 nm Pt/1.9 μm PZT (Zr/Ti = 52/48)/ 200 nm Pt. The dimensions of the PZT membrane and backside cavity are 120 (width) × 500 (length) × 1.9 (thickness) μm^3 and 160 (width) × 550 (length) × 400 (height) μm^3, respectively. The pMUT fabrication process started with a 1 μm SiO_2 layer deposition on an N-type silicon-on-insulator (SOI) wafer for electrical insulation. Then 200 nm Pt/10 nm Ti thin films were deposited by DC magnetron sputtering and patterned as the bottom electrode by Ar ions. A layer of 1.9 μm PZT film was formed using sol-gel process and patterned through wet-etching. Next, another 200 nm Pt/10 nm Ti thin films were deposited and patterned as the top electrode. Last, the Si substrate was etched by deep reaction-ion etching (DRIE) to release the membrane. To functionalize pMUTs, a very simple and versatile drop-casting method was used to deposit pure GO, pure PEI and PEI/GO (PEI v/v = 25%, 50%, 75%) thin films onto the top surface of the pMUT arrays. After deposition, all as-prepared pMUT humidity sensors were placed into the oven and heated at 60 °C for 48 h. The developed TENGs were made of a top suspended PET/Al bilayer and a bottom polytetrafluoroethylene (PTFE)/Al bilayer attached on the flexible PET substrate. An approximately 500 μL of PEI solution with 5% (w/v) concentration was spray-coated on the top Al electrode of a prepared TENG to absorb/desorb CO_2 and heated in a drying oven at 60 °C for 24 h. Hence, the CO_2 concentration can be measured on real time by tracking the change of the triboelectric output. The detailed TENG and PEI-coated TENG structures are shown in Fig. 1c and d. All TENGs operate at the vertical contact-separate mode and share the same effective contact area of 50 × 50 mm^2. After those, the present pMUT array, TENG and PEI-TENG were transferred on the flexible substrate through chip-scale transferring technology (Fig. S1, Supplementary information). The photographs of the as-fabricated individual devices and their integrated multifunctional sensing system are illustrated in Fig. S2 (Supplementary information). For the integration of the system, we leverage this system configuration to validate the feasibility of this hybrid integrated system. In the future, flexible conductive interconnects can be prepared on a flexible substrate, and pMUT chip and other components can be further attached on top using the known flexible electronics technology.

2.2. Working mechanisms of humidity and CO_2 sensors

The flexural resonant frequency of a pMUT humidity sensor has inverse correlation with the surface area of the vibrating membrane and positive correlation with the thickness of the membrane and the ratio of Young's modulus and density [89]. Therefore, coating a selectively sensitive thin film on the pMUT surface could shift the resonant frequency upward or downward, which is depended by the mechanical properties and thickness of the deposited film. Moreover, the physisorption or chemisorption of the analyte molecules on the sensitive thin film would result in a frequency decrease according to the mass-loading effect. The frequency shift of the developed pMUT humidity sensors can be estimated by [90]:

$$\Delta f_0 = -\frac{1}{2} f_0 \times \frac{\Delta m}{m} \quad (1)$$

where m and Δm are the mass of the effective vibration membrane and mass change after absorption of water molecules, respectively. According to the dimensions of the fabricated pMUTs with the working frequencies of approximately 2.58 MHz, the mass sensitivity per unit area is estimated at 16 ag/Hz/μm^2.

To facilitate both good linearity and high sensitivity of pMUT humidity sensors, conventional GO film was modified by PEI polymer and optimized to obtain the best performance. The detailed mechanism of the proposed PEI/GO-coated pMUT humidity sensor is shown in Fig. 2a. The adsorption of water molecules only occurs at the surface and edges of GO sheets and the permeation through the GO sheets is largely restricted due to the 2D honeycomb structure. For pure GO film based sensors, it has been acknowledged that their remarkable nonlinearity at the high RH level (> 60% RH) is resulted from the internal stress induced by the significantly accumulated interlayer expansion [72,76]. Meanwhile, the lag of desorption between the central region and edges of underlying GO sheets would result in a high hysteresis [76]. By contrast, with the participation of PEI film, the GO sheets would be anchored tightly due to the interleaved structure and the formation of the acylamino groups. In this case, the distance between GO sheets in the composite film is enlarged and some effective adsorption/desorption channels could be formed [87], making water molecules quickly penetrate across the whole composite film. Combining with a higher

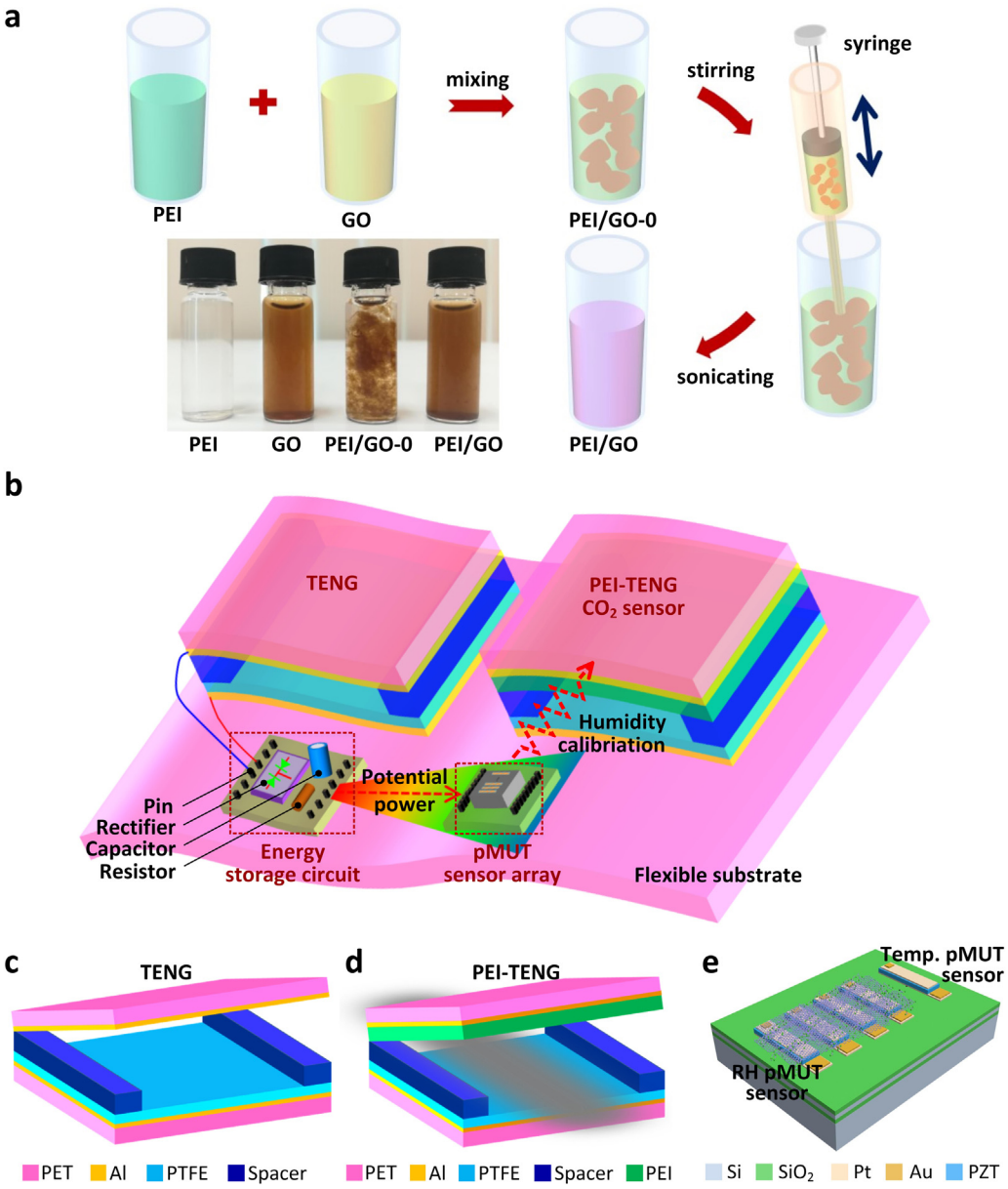

Fig. 1. Schematics and fabrication of the flexible self-powered multifunctional sensing system. (a) Technical route of preparing the PEI/GO composite thin film. (b) Schematic illustration of the flexible self-powered multifunctional sensing system. Structural configurations of (c) the TENG energy harvester, (d) the PEI-TENG CO_2 gas sensor and (e) the linear pMUT array based humidity sensor and temperature sensor.

surface area of PEI/GO composite film, it is promising that the PEI/GO-pMUT exhibits an enhanced sensitivity at a low RH level. With the increase of humidity, water molecules would continuously diffuse into the underlying layers via the adsorption channels. Considering the anchoring of GO sheets and electrostatic interaction between positively charged amine groups from PEI and negatively charged hydroxyl groups from GO, the interlayer expansion effect of composite layer is highly suppressed, leading to a stable and rapid adsorption. When the humidity further increases and reaches to a high level, the swelling effect of the PEI/GO composite film would become nonnegligible. However, owing to the cooperative effect of the chemical bonding (acylamino) and electrostatic interaction, the interlayer expansion of the PEI/GO composite film would be suppressed to some extent compared with the pure GO film. As a result, the swelling effect will be compromised and induce a diminished internal stress in the PEI/GO film, only making for a slight increase in the frequency shift of PEI/GO-pMUT. When it comes to the dehumidification, the internal water molecules could be effectively released through the desorption channels in the similar way. Therefore, the optimized PEI/GO composite film could qualify the pMUT with an excellent humidity-sensing performance, such as high sensitivity, good linearity, small hysteresis and little energy loss.

The working principle of the PEI-TENG in one cycle of contact and separation and the underlying CO_2 sensing mechanism are illustrated in Fig. S3 (Supplementary information). PEI-TENG has CO_2 gas sensing response due to the chemical reactions between CO_2 and the amine groups of the branched PEI polymer chain and corresponding electroconductivity change during the CO_2 adsorption. The involved chemical reactions are as below

$$CO_2 + 2R_1NH_2 \rightleftharpoons R_1NHCOO^- + R_1NH_3^+ \quad (2)$$

$$CO_2 + 2R_2NH \rightleftharpoons R_2NCOO^- + R_1NH_2^+ \quad (3)$$

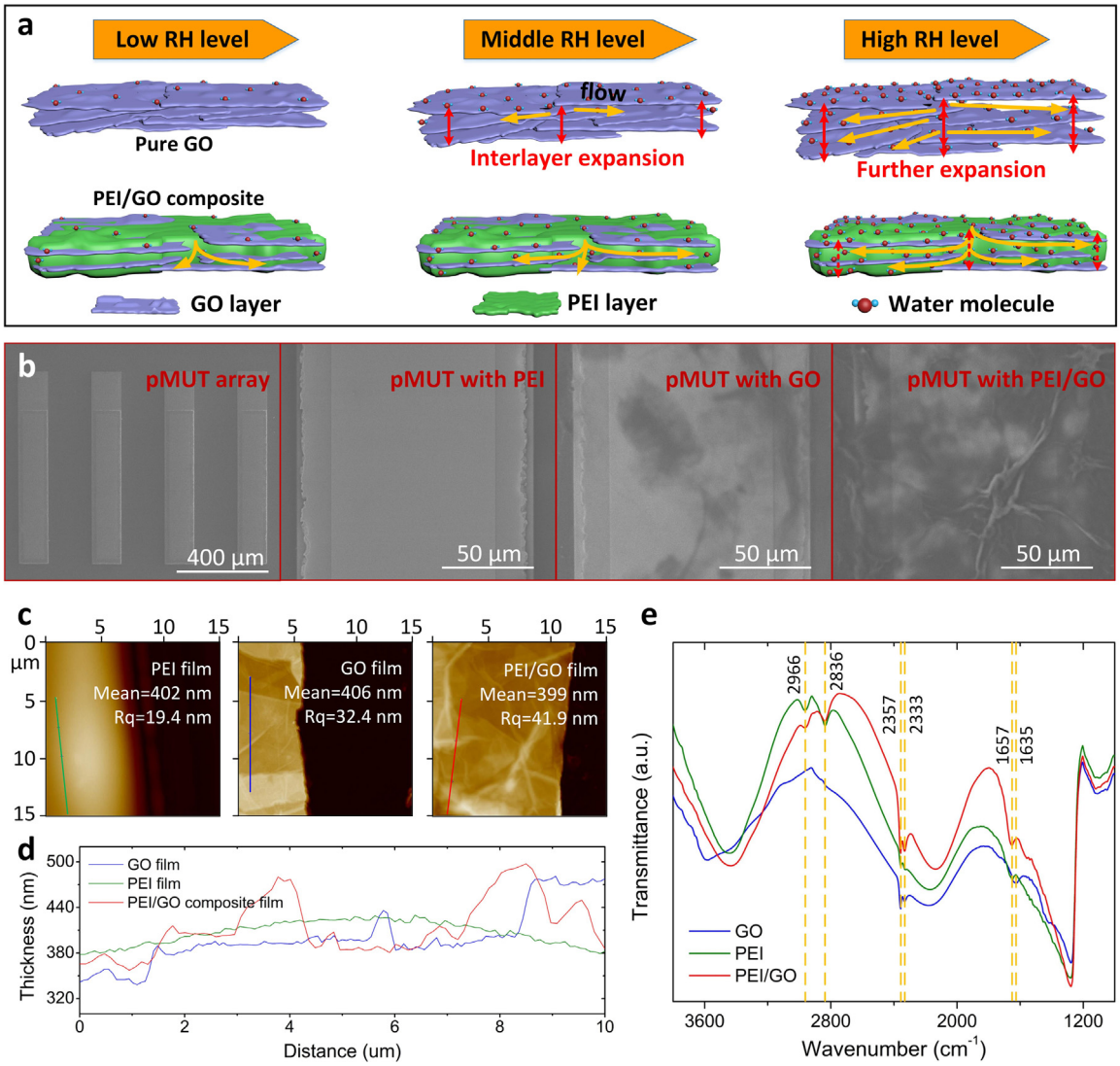

Fig. 2. Humidity sensing mechanism and material characterization. (a) Humidity-sensing mechanism of the PEI/GO-pMUT humidity sensor. (b) SEM images of the pMUT array before functionalization and the pMUTs after deposition of PEI, GO and PEI/GO films. (c) AFM image. (d) Height profile analysis and (e) FTIR spectra of the deposited PEI, GO and PEI/GO films.

$$CO_2 + R_1NH_2 + R_2NH \rightleftharpoons R_2NCOO^- + R_1NH_3^+ (\text{or } R_1NHCOO^- + R_2NH_2^+) \quad (4)$$

Once PEI-TENG is exposed to CO_2 atmosphere, CO_2 molecules are easily absorbed onto the PEI film surface to extract electrons from N—H sites of PEI polymer and PEI will be protonated to form N^+—H bonds, resulting in the formation of a carbamate layer [91]. In this process, the electroconductivity of PEI is increased and the induced charge from the electrification between the Al/PEI and PTFE will be enlarged. When PEI with N^+—H sites is exposed to air or CO_2 atmosphere with a lower concentration again, CO_2 would be desorbed and protonated PEI is transformed to its original form again. The whole CO_2 adsorption/desorption process is reversible so that the electroconductivity of PEI could be also reversible and has a significant impact on the electron transport and the output performance of the TENG. By monitoring the induced charge change of the PEI-TENG, different CO_2 concentrations could be detected timely.

2.3. Measurement and characterization

The surface morphologies of the pMUT humidity sensors before and after coating GO, PEI, PEI/GO thin films were characterized by high resolution field emission scanning electron microscope (FEI Nova NanoSEM 230) operated at 15 kV. Atomic force microscopy (Bruker Dimension FastScan AFM) was used to investigate the thickness and roughness of GO, PEI and PEI/GO films coated on the pMUTs. To acquire the chemical information of the GO, PEI and PEI/GO films, a high-resolution FTIR spectroscopy (Agilent Technologies Cary 600 Series) was deployed at the transmission mode. The real-time output charge, current and voltage of under-test TENG and PEI-TENG were measured by Keithley 6514 system electrometer with a SR570 low-noise current preamplifier (Stanford Research Systems) and recorded by a personal computer (PC). During the measurements, a precision impedance analyser (Agilent 4294 A) was used to measure the resonant frequency of the pMUT humidity sensors and the concentration of CO_2 gas was measured by a commercial GCH-2018 carbon oxide/humidity/temperature meter (Lutron Company, Taiwan).

Fig. 2b shows the SEM images of untreated pMUT array and functionalized pMUT humidity sensors. The pure PEI film coated pMUTs have a flat surface whereas the PEI/GO pMUTs exhibit remarkable ripples and wrinkles. To acquire the same thickness for all deposited films, we firstly investigated the thickness dependence of the GO and

PEI films on the concentrations of their dilution dispersions, as shown in Fig. S4 (Supplementary information). After optimizing concentrations of PEI and GO dispersions to 0.375% (w/v) and 1 mg/L, respectively, the similar thickness of 400 nm for PEI, GO and PEI/GO films were achieved. The AFM images and corresponding height profile analyses of all pMUT samples are depicted in Figs. 2c and 2d, where the mean thickness of GO, PEI and PEI/GO films is 406 nm, 402 nm, and 399 nm, respectively. However, a remarkable difference in root-mean-square (RMS) among the surfaces of these films shows that the accessible surface area of GO film has been enhanced after modification with PEI polymer. Fig. 2e displays the FTIR spectra of the prepared pure GO, pure PEI and hybrid PEI/GO films. The strong resonance peaks at 2966 cm^{-1} and 2836 cm^{-1} observed in PEI and PEI/GO films should be correlated to asymmetric and symmetric stretching modes of $-CH_2-$ groups. The weakened intensity in PEI/GO composite is attributed to halved PEI volume compared with pure PEI film. Meanwhile, another two peaks at 2357 cm^{-1} and 2333 cm^{-1} appeared in all three films, corresponding to the formation of unique chemical species in the presence of CO_2 [92]. It is worth noting that the existence of peak at 1657 cm^{-1} (C=O of acylamino groups) in PEI film results from the absorption of CO_2 and its involved chemical reactions with amine groups. An almost complete disappearance of peak at 1635 cm^{-1} (C=O of carboxyl groups) that is only found in GO film and an enhanced peak at 1657 cm^{-1} in PEI/GO composite suggests the effective amidation reaction between the carboxyl groups in GO film and amine groups in PEI film.

3. Results and discussion

The finite element method (FEM) based on COMSOL Multiphysics v5.2a was utilized to preliminarily determine the fundamental frequencies of pMUTs. Then a precision impedance analyser Agilent 4294 A was used to record the impedance and phase curves of the pMUT humidity sensors before and after coating GO, PEI, and 50% (v/v) PEI/GO films. The simulated and tested frequency responses are shown in Fig. S5 (Supplementary information). Due to the very low mechanical modulus of PEI film, the working frequency of PEI-pMUT was shifted slightly down by 1.7 kHz. In contrast, the deposited GO and PEI/GO films increase the resonant frequency by 72.85 kHz and 31.80 kHz, respectively, mainly owing to the increased thickness and comparable ratio of Young's modulus and density. Compared with GO-pMUT, the approximately halved frequency change of PEI/GO-pMUT indicates the equivoluminal mixing between PEI and GO films. The detailed information of as-fabricated pMUT humidity sensors was summarized in Table S1 (Supplementary information).

The experimental setup for humidity-sensing property measurement is illustrated in Fig. 3a. The pMUT humidity sensors were switchably placed in one of two sealed plastic chambers. P_2O_5 desiccant and humidifier with DI water were used together to obtain RH levels from 10% to 90% with a 10% RH interval. The relative humidity in the chambers was manually changed by adjusting the flow rate of the evaporative moistures and recorded in real time by a precise relative humidity meter. The temperature in the test chamber was controlled by combining the hotplate and indoor air conditioner to achieve the range from 20 to 50 °C. During the humidity measurement, the temperature in the chamber was kept constant at 24 ± 0.5 °C to eliminate the interference from temperature changes. The modulation effect of the PEI component in the PEI/GO composite on the humidity-sensing performance of the pMUT sensor was firstly investigated in terms of its volume fraction, as shown in Fig. 3b, where the total thickness of the composite film was kept the same. It is demonstrated that the linear sensing range only occurs in the high RH range (> 50%) when the PEI volume fraction is less than 50% (v/v), while the lower limit of the linear range will be extended to a lower RH level with a cut-down sensitivity when the PEI volume fraction is higher than 50% (v/v). Therefore, the PEI volume fraction of the PEI/GO composite film was optimized to 50% (v/v) for the best humidity-sensing properties including sensitivity and linearity. In all following experiments, 50% (v/v) PEI/GO composite film was applied on the pMUT for further investigation in terms of both humidity and temperature responses.

Fig. 3c illustrates the temperature responses of the pMUT sensors without and with functionalization of the PEI/GO composite film, where the humidity was kept constant at 10% RH. It is clearly shown that the resonant frequency decreases linearly with the temperature increasing. The temperature coefficients of frequency (TCFs) of the pMUTs without and with the PEI/GO composite film are −36.3 ppm/°C and −98.1 ppm/°C, respectively. It is worth noting that the relatively significant temperature impact on the resonant frequencies of the PEI/GO-pMUT can be easily compensated by employing some pMUT elements without the functionalization as the reference sensors to detect the temperature change owing to the multi-pMUT array structure, which is much more advantageous than other resonators. The humidity response of the reference pMUT temperature sensor is shown in Fig. S6 (Supplementary information), offering a reasonable linearity in the humidity range from 10% to 90% RH. When the pMUT without any functional film is adopted as the temperature sensor, the sensitivity and limit of detection (LOD) of the temperature response are 90 Hz/°C and 0.72 °C, respectively.

The steady frequency shifts of three pMUT sensors (GO-pMUT, PEI-pMUT and PEI/GO-pMUT) are plotted in Figs. 3d and 3e. It is clearly shown that there is a good frequency stability within each RH level for all sensors. As the RH level increases, the resonant frequency steps down, which is consistent with the mass-loading effect. The GO-pMUT exhibits a remarkable nonlinear response with RH levels, as reported in previous publications [72,77,87]. In contrast, the PEI-pMUT has a very good linear behaviour in the RH range from 30% to 80%. In particular, the PEI/GO-pMUT presents an impressive linearity with RH levels of 20–90% and a slight improvement in the frequency shift at 90% RH, indicating the humidity-sensing superiority of PEI/GO composite thin film. The regression-square coefficient (R^2) of the linear fitting curve for PEI/GO-pMUT is 0.99507 (Fig. 3e). The linearity characteristic of PEI/GO-pMUT could be attributed to the modulation of PEI component on the interlayer distance of the GO sheets. The average sensitivities of three humidity sensors in the RH range of 10–90% are calculated as 719.37 Hz/% RH for GO-pMUT, 543.75 Hz/% RH for PEI-pMUT, and 748.12 Hz/% RH for PEI/GO-pMUT, which are at least one order higher than previously reported QCM based humidity sensors [72,73,80]. A humidity-sensing sensitivity comparison between our developed pMUT sensors and other reported resonant sensors is listed in Table 1. It is confirmed that the pMUT humidity sensors have outstanding humidity-sensing property with high sensitivity (S_{rh}) and relative sensitivity (S_{rh}/f_0).

The hysteresis characteristics of three pMUT sensors were studied, as shown in Fig. 4a. The hysteresis of all sensors is calculated as 3.95% RH for GO-pMUT, 2.87% RH for PEI-pMUT and 3.07% RH for PEI/GO-pMUT. After 50% (v/v) PEI modification on GO film, the PEI/GO composite coated sensor exhibits a lower hysteresis than pure GO film coated sensor. When the RH level in the chamber returns to 10%, the hysteresis is nearly disappeared. To investigate dynamic response and recovery characteristics of PEI/GO-pMUT, two chambers were kept at 23% and 62% RH levels, respectively. The pMUT sensors were manually transferred from one to the other chamber alternatively for four cycles. It took about 2 s to transfer the pMUT devices. Fast moisture adsorption/desorption and excellent repeatability were observed in Fig. 4b. The average response and recovery time (reaching 90% of the final value) of the PEI/GO-pMUT for four cycles is 22 s and 53 s. It is worth mentioning that the theoretical recovery time should be shorter than the tested result because the RH level has been slightly increased by about 5% RH after quickly opening the chamber and then gradually brought back to 23% RH due to the existence of P_2O_5 desiccant.

The frequency stability including short-term stability and long-term stability is an important parameter for the humidity sensing

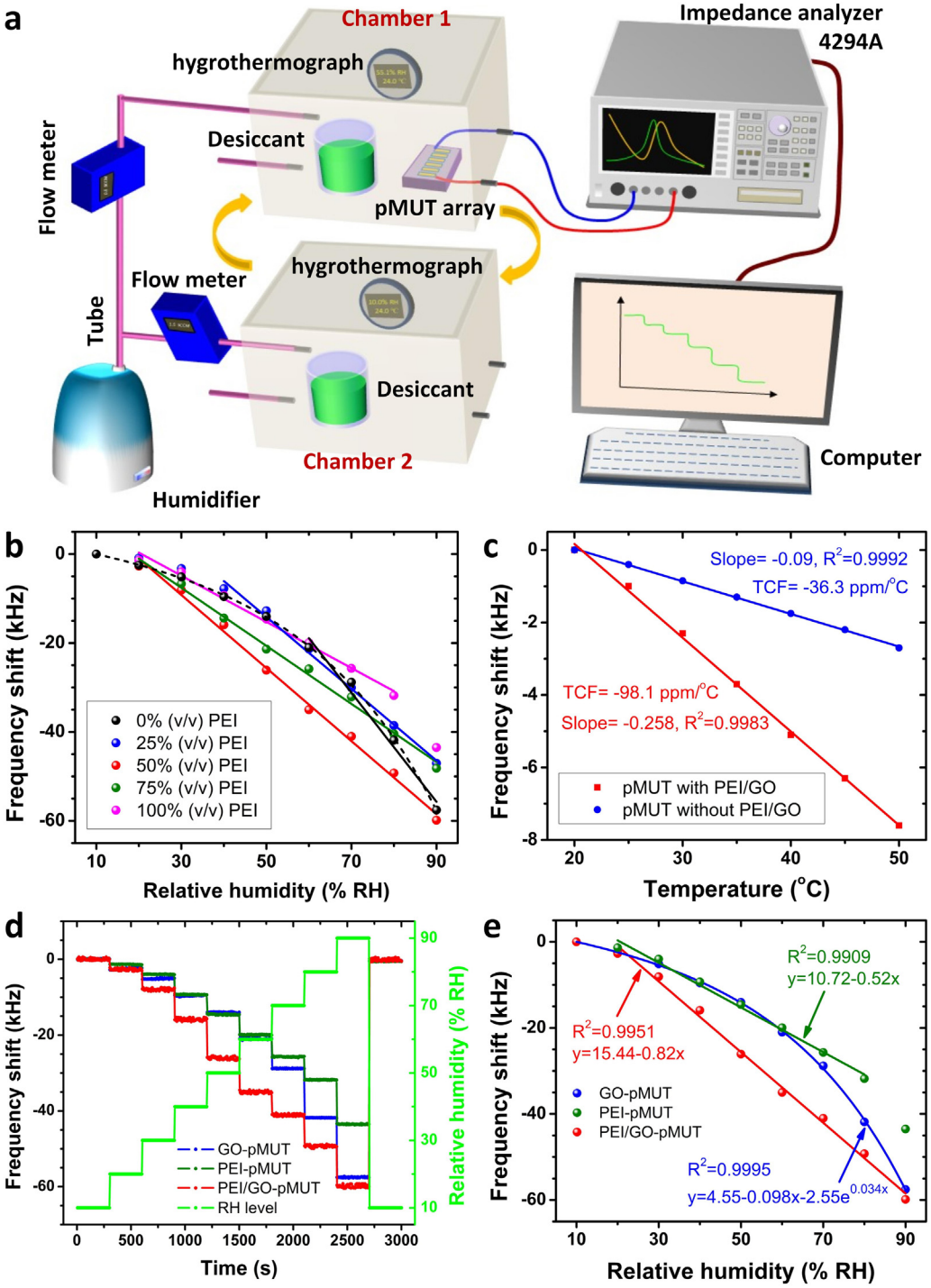

Fig. 3. Temperature and RH sensing by the pMUTs. (a) Modulation effect of PEI volume fractions on the humidity-sensing responses of the PEI/GO composite coated pMUTs. (b) Frequency dependence on temperature for the pMUTs without and with functionalization of 50% (v/v) PEI/GO composite film. (c) Steady frequency responses of three pMUT humidity sensors. (d) Relation between the frequency shift and RH levels.

measurement. The short-term stability can be expressed as an Allan deviation, i.e. sigma-tau σ(τ), to estimate the noise Δf and the LOD of the sensor [63]. The average overlapped Allan deviations measured under various RH levels are 95 Hz (1σ) for GO-pMUT, 64 Hz (1σ) for PEI-pMUT and 240 Hz (1σ) for 50% (v/v) PEI/GO-pMUT. Thus, the humidity detection limits of these three sensors are 0.40% RH (3σ), 0.35% RH (3σ) and 0.96% RH (3σ), all of which are better than 1% RH. The long-term stability for the optimized PEI/GO-pMUT humidity sensor was verified by monitoring its resonant frequency at 20%, 40%, 60% and 80% RH levels per 4 days for 1 month, as shown in Fig. 4c. There is only a little fluctuation at middle RH levels, indicating a good consistency. It is worth mentioning that when these pMUT humidity sensors were exposed to CO_2 atmosphere with concentration up to 20,000 ppm, there was no noticeable frequency change (< 250 Hz), demonstrating that all pMUT sensors have excellent selection for water molecules over CO_2 gas.

The impedance and phase response spectra of three pMUT sensors under various RH levels were recorded in Fig. 5a-f. It is observed that not only the frequencies in the impedance response but also the frequencies in the phase response are shifted downward for all sensors as

Table 1
Comparison of pMUT humidity sensors and other reported resonant sensors.

Devices	Sensing material	f_0 (MHz) @10% RH	Sensing range (% RH)	S_{rh} (kHz /% RH)	S_{rh}/f_0 (ppm /% RH)
SAW [59]	Sol-gel SiO_2	199.3	30–93	8.254	41.41
SAW [77]	GO	392	10–90	11.61	29.62
FBAR [60]	ZnO	1431.165	22–82	8.5	5.94
FBAR [93]	GO	1247	0–83	6.6265	5.31
Cantilever [62]	GO	2.12	10–90	0.13125	61.91
cMUT [63]	Mesoporous silica	47.4	0–80	2.19	46.2
QCM [73]	GO/SnO_2/PANI	8	0–97	0.0291	3.64
QCM [80]	P-PEI-GO	10	11.3–97.3	0.0191	1.91
pMUT	GO	2.65285	10–90	0.71937	271.17
pMUT	PEI	2.5833	10–90	0.54375	210.49
pMUT	PEI/GO	2.5793	10–90	0.74812	290.05

the RH level increases. The phase peaks show a small degradation when the RH level is increased from 10% to 60% and a remarkable improvement when the RH level is consistently increased to 90%. The change in the first stage could be caused by water molecules mass load and the increased viscosity of the sensing film while the second-stage change could be interpreted as the large interlayer expansion of the sensing film after absorbing abundant moistures. When the driving peak-to-peak voltage for the pMUT sensors is cut down to 100 mV from 1 V during the impedance measurement, the output response still behaves well with little noise interference and good signal-to-noise ratio (SNR). Considering that the effective impedance of the pMUT sensors at the fundamental resonance mode ranges from 150 to 165 Ω, the power consumption of one pMUT sensor can be estimated to be less than 67 μW. To characterize the energy conversion efficiency of three functionalized pMUT sensors, the relative electromechanical coupling coefficient (K_{rt}^2) is defined as the ratio of the electromechanical coupling coefficients of the pMUT sensor before and after functionalization. Fig. 4d plots the K_{rt}^2 of three pMUT humidity sensors under different RH levels. Both the GO-pMUT and PEI-pMUT sensors exhibit a noticeable increasing trend of K_{rt}^2 coefficient at the RH level lower than 60%. This can be caused by an increase in viscoelasticity of the sensitive film after a small amount of water adsorption [94], which is consistent with the aforementioned explanation in the first stage. As a comparison, the PEI/GO-pMUT sensor possesses a more stable K_{rt}^2 coefficient in a wide RH range from 10% to 70% owing to the chemical amidation reaction in PEI/GO composite film, indicating less energy loss and more effective sensing in humidity. When the sensors operate at the high RH levels, the swelling effect of sensitive film becomes dramatical due to the formation of a continuous water phase throughout the film [95], resulting in a large interlayer expansion and in turn leading to a small reduction of the K_{rt}^2 coefficient.

Fig. 6a elucidates the testing setup for exploring the TENG-based energy harvesting behaviors. The assembled TENG with effective friction contact area of 50 × 50 mm^2 was operated by a linear motorized force gauge tester (Force Mecmesin ILC-S 2500 N) to simulate the mechanical energy in ambient. The force gauge tester mainly contains a digital force gauge, a linear guiderail, a moving stage and a fixed platform. The TENG device is attached on the fixed platform. The moving stage periodically approaches and moves apart from the device at the frequency of 1.5 Hz. Through the test, the induced charge, short-circuit current, output voltage of the TENG are shown in Fig. 6b–d. It is seen that the peak-to-peak values of short-circuit current and output voltage are 22.5 μA and 1050 V, respectively. To investigate the resistance load matching characteristic and output power capability of the as-fabricated TENG, both the output voltage and power were measured under different external resistance from 100 kΩ to 100 MΩ, as illustrated in Fig. 6e. The inset describes the measurement diagram of the electric output circuit. The output voltage keeps going up to a stable level with the resistance load increasing, while the output peak power holds a maximal value of 7.5 mW at a loading resistance of

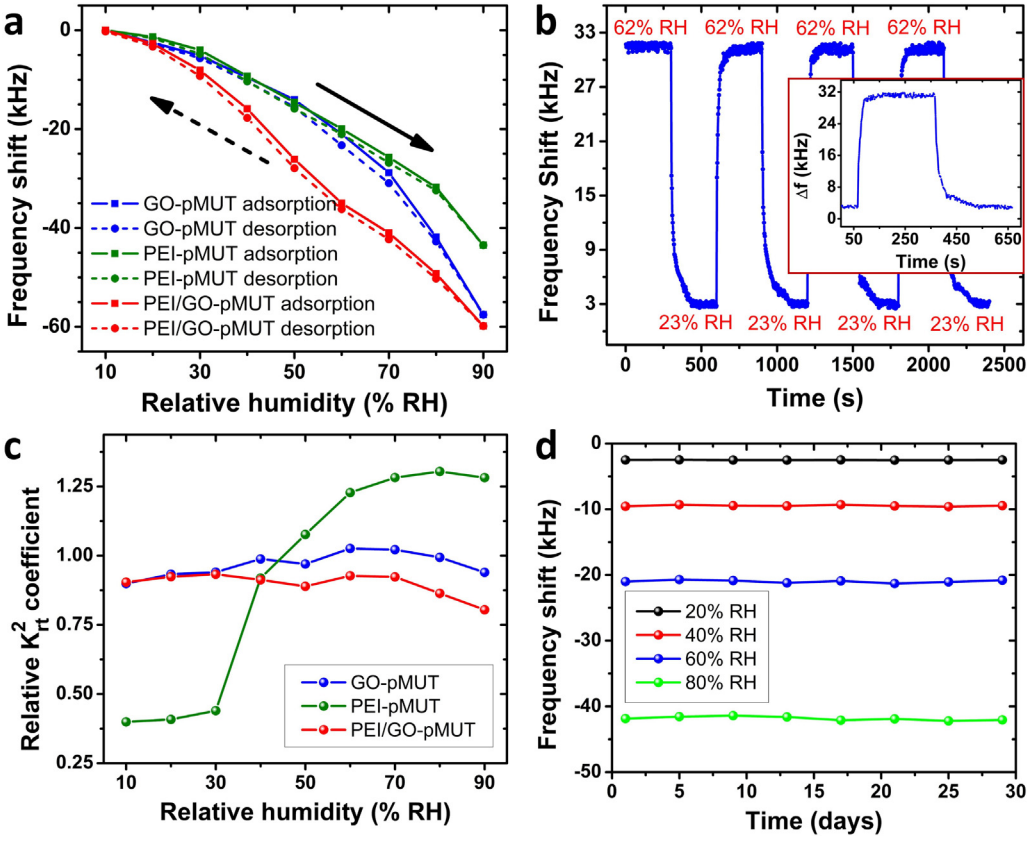

Fig. 4. Detail characterization of the pMUTs for RH sensing. (a) Hysteresis property of three pMUT humidity sensors. (b) Repeatability of PEI/GO-pMUT with four cycles. (c) Relative electromechanical coupling efficient of three pMUT sensors versus relative humidity. (d) Long-term stability of PEI/GO-pMUT sensor at various RH levels for 1 month.

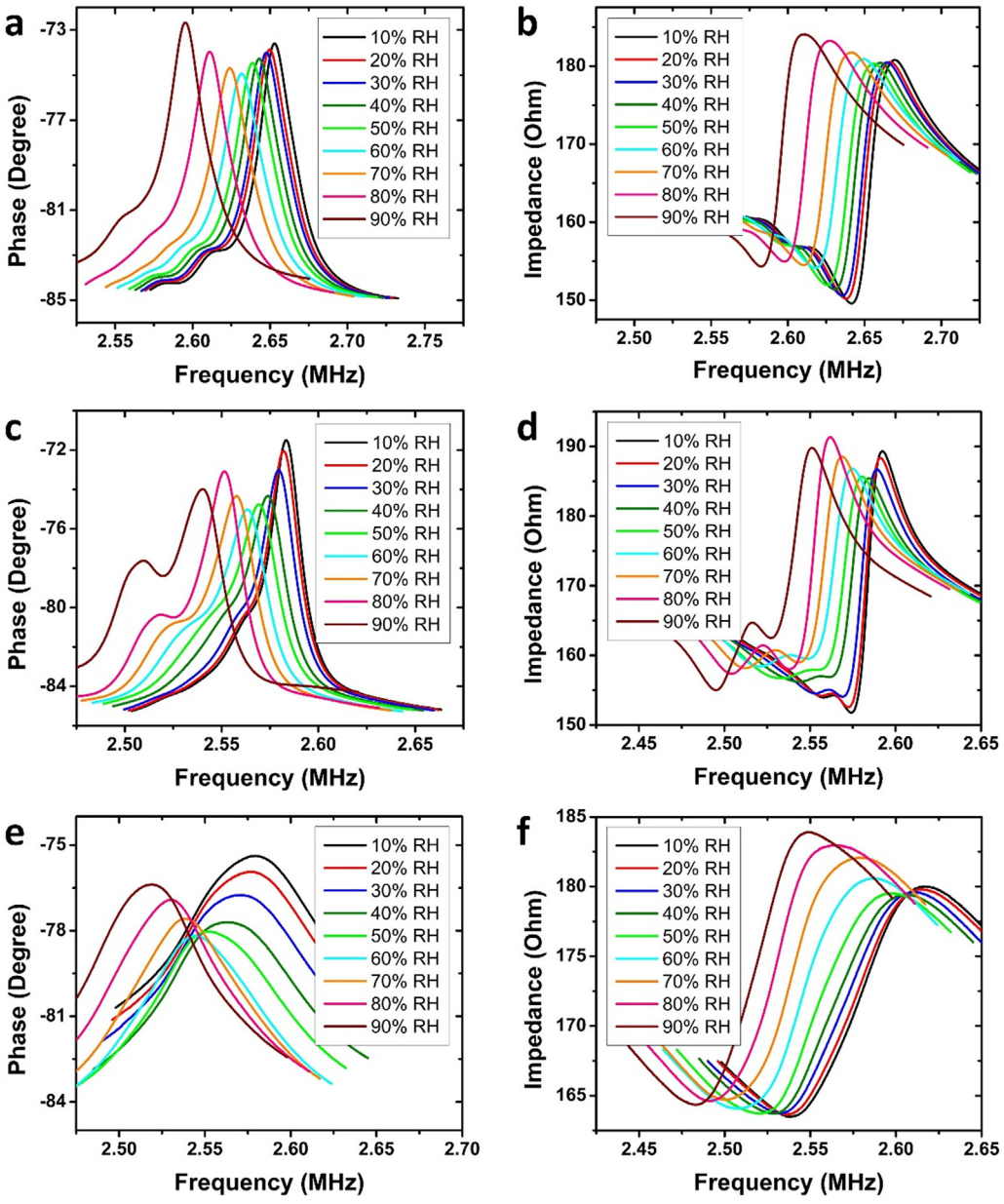

Fig. 5. Impedance and phase spectra of pMUT humidity sensors under various RH levels. (a) Phase curves and (b) impedance spectra of GO-pMUT humidity sensor. (c) Phase curves and (d) impedance spectra of PEI-pMUT humidity sensor. (e) Phase curves and (f) impedance spectra of PEI/GO-pMUT humidity sensor.

15.3 MΩ. Such power is typically sufficient to drive most microfabricated sensors including our developed pMUT sensors with the power consumption of about 70 μW. To efficiently collect and reuse the generated triboelectric energy, a full-wave rectifier bridge is applied to convert the alternating electric signals to unipolar-pulsing DC (direct current) output and then connected with a storage capacitor. The TENG device is tested for charging three different values of capacitors (1 μF, 4.7 μF and 47 μF). The relation between the output voltage and charging time is shown in Fig. 6f. The potentials on the storage capacitors after 60 s charging are 22.8 V for 1 μF capacitor, 7.13 V for 4.7 μF capacitor and 1.25 V for 47 μF capacitor. Therefore, the harvested energy can be potentially used to periodically supply miniaturized sensors with sub-milliwatt power consumption.

The CO_2 sensing performance of PEI-TENG was investigated by exposing the sensor to various CO_2 concentrations in a wide range from about 600 to over 12,000 ppm. The relative humidity level in the test chamber was firstly kept constant to exclude its impacts on induced charge. Fig. 6g presents the experimental setup of the PEI-TENG based CO_2 sensor and the measured response is shown in Fig. 6h. It is obviously seen that the generated charge of the sensor monotonically increases with the CO_2 concentration increasing from 684 to 12,735 ppm, resulting from the increase in electroconductivity of PEI film. The results demonstrate the protonation effect of PEI film upon exposure to CO_2 atmosphere with higher concentrations, which is consistent with the previous CO_2 sensing mechanism analysis. After adequate adsorption of CO_2 molecules, the output charge maintains at a relative stable level. Fig. 6i reveals the charge transfer curves under different CO_2 concentrations and relative humidity levels. Though the curves of three different RH levels (56%, 65% and 83%) show the similar increasing trend as the CO_2 concentration rises up, the lower RH can generate a higher transferred charge, indicating that relative humidity has a nonnegligible and detrimental impact on the performance of the Al/PEI-PTFE TENG sensor [96]. Thus, with the detection and calibration of the relative humidity by the present PEI/GO-pMUT sensors, the PEI-TENG is promising to provide a precise measurement for CO_2 gas (Fig. S7, Supplementary information).

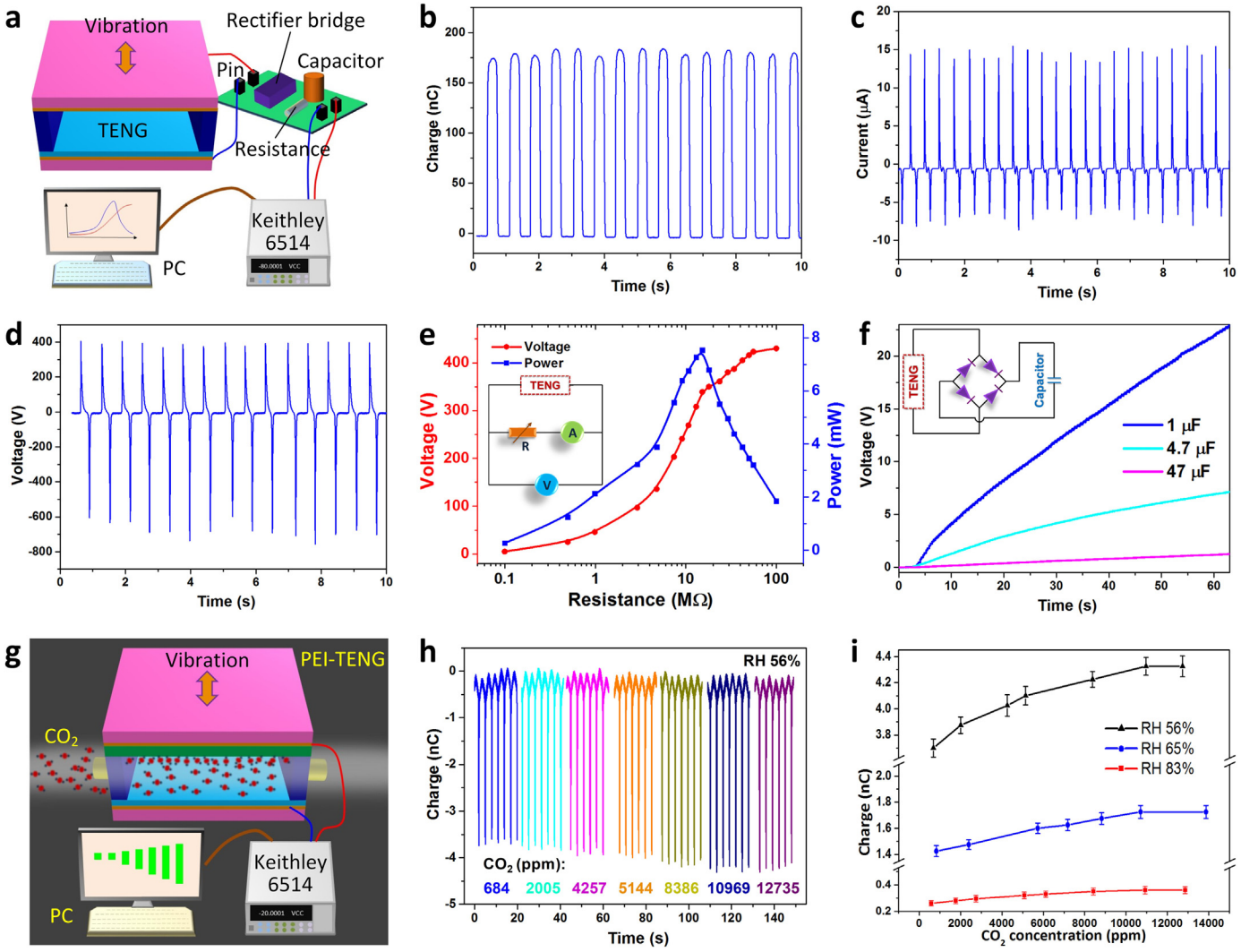

Fig. 6. Energy harvesting and CO_2 sensing by TENGs. (a) Testing setup for exploring the TENG-based energy harvesting behaviors. (b) The output charge, (c) output current and (d) output voltage of the prepared TENG. (e) Dependence of the output voltage and power on the external resistance load. Insert: the measurement circuit diaphragm. (f) Charging curves of 1 μF, 4.7 μF and 47 μF capacitors by TENG. Insert: the measurement circuit diaphragm. (g) Experimental setup of the PEI-TENG based CO_2 sensing measurement. (h) Output charge response under various CO_2 concentrations. (i) Dependence of the response-concentration curves on RH levels.

4. Conclusion

In summary, a self-powered flexible multifunctional monitoring microsystem based on two TENGs and a microstructured pMUT array has been designed for harvesting the mechanical energy and simultaneously detecting CO_2 gas, relative humidity and room temperature. With the PEI film coating, one TENG is functionalized as the self-powered active CO_2 gas sensor and characterized under various CO_2 concentrations and RH levels. The prepared TENG-based gas sensor possesses a good CO_2-sensing response with a wide detection range from below 700 ppm to over 12,000 ppm. Meanwhile, with the other TENG as potential power supply, a linear pMUT array is used to simultaneously detect relative humidity and room temperature by employing some pMUT elements as the humidity sensors and the others as the temperature sensors. A PEI/GO composite film with an optimized PEI volume fraction is coated on the pMUT humidity sensor to obtain ultrasensitive and linear humidity-sensing properties. The results show that the developed humidity sensor has an extremely high sensitivity (748 Hz/% RH) and relative sensitivity (290 ppm/% RH), rapid response and recovery (< 22 s/53 s @ 90%), small hysteresis (3.07% RH), excellent linearity over a wide range of 20–90% RH (0.9951 for R^2) and good stability. The present pMUT temperature sensor exhibits an excellent linear response with TCF of −36.3 ppm/°C, which could be further utilized to calibrate the temperature effect of humidity sensors due to the shared pMUT array structure. In addition, both the CO_2-sensing and humidity-sensing mechanisms are explored and discussed. This study not only provides a novel strategy of integrating multiple miniaturized sensors with TENG devices for low-cost, high-efficiency, flexible and multifunctional self-powered electronics, but also creates an effective route of utilizing the functionalized pMUT array to facilitate both ultrasensitive and linear humidity detection.

Acknowledgement

This work was supported by the HIFES grant project “Hybrid Integration of Flexible Power Source and Pressure Sensors” (Grant no. R263501012133), the A*STAR-NCBR grant project “Chip-Scale MEMS Micro-Spectrometer for Monitoring Harsh Industrial Gases” (Grant no. R263000C91305), the Fundamental Research Funds for the Central Universities (Grant nos. 106112015CDJXY120007, 106112017CDJQJ118846, 106112017CDJXSJW0007 and 10611CDJXZ238826) and the National Key Research and Development Program of China (Grant nos. 2016YFE0125200 and 2016YFC0101100). This work was also supported by the China

Scholarship Council (CSC). Changhe Sun would like to thank Ms. Fujun Sun for assistance with AFM measurements and precious encouragement during NUS study.

Appendix A. Supplementary material

Supplementary data associated with this article can be found in the online version at doi:10.1016/j.nanoen.2019.01.096.

References

[1] Z.L. Wang, Sci. Am. 298 (2008) 82–87.
[2] Z.L. Wang, Mater. Today 20 (2017) 74–82.
[3] M. Ha, J. Park, Y. Lee, H. Ko, ACS Nano 9 (2015) 3421–3427.
[4] P.K. Yang, L. Lin, F. Yi, X. Li, K.C. Pradel, Y. Zi, C.I. Wu, J.H. He, Y. Zhang, Z.L. Wang, Adv. Mater. 27 (2015) 3817–3824.
[5] H. Ouyang, J. Tian, G. Sun, Y. Zou, Z. Liu, H. Li, L. Zhao, B. Shi, Y. Fan, Y. Fan, Z.L. Wang, Z. Li, Adv. Mater. 29 (2017) 1703456.
[6] H. Feng, C. Zhao, P. Tan, R. Liu, X. Chen, Z. Li, Adv. Healthc. Mater. 7 (2018) 1701298.
[7] B. Shi, Z. Li, Y. Fan, Adv. Mater. 30 (2018) 1801511.
[8] W. Jiang, H. Li, Z. Liu, Z. Li, J. Tian, B. Shi, Y. Zou, H. Ouyang, C. Zhao, L. Zhao, R. Sun, H. Zheng, Y. Fan, Z.L. Wang, Z. Li, Adv. Mater. 30 (2018) 1801895.
[9] B.C. Tee, A. Chortos, A. Berndt, A.K. Nguyen, A. Tom, A. McGuire, Z.C. Lin, K. Tien, W.G. Bae, H. Wang, P. Mei, H.H. Chou, B. Cui, K. Deisseroth, T.N. Ng, Z. Bao, Science 350 (2015) 313–316.
[10] X. Wang, Y. Gu, Z. Xiong, Z. Cui, T. Zhang, Adv. Mater. 26 (2014) 1336–1342.
[11] C. Wang, X. Li, E. Gao, M. Jian, K. Xia, Q. Wang, Z. Xu, T. Ren, Y. Zhang, Adv. Mater. 28 (2016) 6640–6648.
[12] S. Han, J. Kim, S.M. Won, Y. Ma, D. Kang, Z. Xie, K.T. Lee, H.U. Chung, A. Banks, S. Min, S.Y. Heo, C.R. Davies, J.W. Lee, C.H. Lee, B.H. Kim, K. Li, Y. Zhou, C. Wei, X. Feng, Y. Huang, J.A. Rogers, Sci. Transl. Med. 10 (2018) eaan4950.
[13] W. Gao, S. Emaminejad, H.Y.Y. Nyein, S. Challa, K. Chen, A. Peck, H.M. Fahad, H. Ota, H. Shiraki, D. Kiriya, D.H. Lien, G.A. Brooks, R.W. Davis, A. Javey, Nature 529 (2016) 509–514.
[14] Y. Zi, Z.L. Wang, APL Mater. 5 (2017) 074103.
[15] X. Cao, Y. Jie, N. Wang, Z.L. Wang, Adv. Energy Mater. 6 (2016) 1600665.
[16] L. Yang, Z.G. Chen, M.S. Dargusch, J. Zou, Adv. Energy Mater. 8 (2018) 1701797.
[17] F.D. Giacomo, A. Fakharuddin, R. Jose, T.M. Brown, Energy Environ. Sci. 9 (2016) 3007–3035.
[18] C. Sun, Y. Wen, P. Li, W. Ye, J. Yang, J. Qiu, J. Wen, IEEE Trans. Mag. 52 (2016) 8600204.
[19] Z.L. Wang, Nanogenerators for Self-Powered Devices and Systems, Georgia Institute of Technology, Atlanta, USA, 2011 (ISBN 978-1-4507-8016-2).
[20] F.R. Fan, Z.Q. Tian, Z.L. Wang, Nano Energy 1 (2012) 328–334.
[21] Z.L. Wang, ACS Nano 7 (2013) 9533–9557.
[22] R. Hinchet, W. Seung, S.W. Kim, ChemSusChem 8 (2015) 2327–2344.
[23] J.W. Lee, B.U. Ye, J.M. Baik, APL Mater. 5 (2017) 073802.
[24] X.S. Zhang, M. Han, B. Kim, J.F. Bao, J. Brugger, H. Zhang, Nano Energy 47 (2018) 410–426.
[25] X. Pu, L. Li, H. Song, C. Du, Z. Zhao, C. Jiang, G. Cao, W. Hu, Z.L. Wang, Adv. Mater. 27 (2015) 2472–2478.
[26] Q. Jiang, C. Wu, Z. Wang, A.C. Wang, J.H. He, Z.L. Wang, H.N. Alshareef, Nano Energy 45 (2018) 266–272.
[27] S.F. Leung, K.T. Ho, P.K. Kung, V.K.S. Hsiao, H.N. Alshareef, Z.L. Wang, J.H. He, Adv. Mater. 30 (2018) 1704611.
[28] L. Zhao, Q. Zheng, H. Ouyang, H. Li, L. Yan, B. Shi, Z. Li, Nano Energy 28 (2016) 172–178.
[29] P.K. Yang, Z.H. Lin, K.C. Pradel, L. Lin, X. Li, X. Wen, Z.L. Wang, ACS Nano 9 (2015) 901–907.
[30] F. Yi, L. Lin, S. Niu, P.K. Yang, Z. Wang, J. Chen, Y. Zhou, Y. Zi, J. Wang, Q. Liao, Y. Zhang, Z.L. Wang, Adv. Funct. Mater. 25 (2015) 3688–3696.
[31] H. Guo, M.H. Yeh, Y.C. Lai, Y. Zi, C. Wu, Z. Wen, C. Hu, Z.L. Wang, ACS Nano 10 (2016) 10580–10588.
[32] J. Chen, J. Yang, Z. Li, X. Fan, Y. Zi, Q. Jing, H. Guo, Z. Wen, K.C. Pradel, S. Niu, Z.L. Wang, ACS Nano 9 (2015) 3324–3331.
[33] Q. Shi, H. Wang, H. Wu, C. Lee, Nano Energy 40 (2017) 203–213.
[34] Y. Xi, H. Guo, Y. Zi, X. Li, J. Wang, J. Deng, S. Li, C. Hu, X. Cao, Z.L. Wang, Adv. Energy Mater. 7 (2017) 1602397.
[35] Y. Yang, G. Zhu, H. Zhang, J. Chen, X. Zhong, Z.H. Lin, Y. Su, P. Bai, X. Wen, Z.L. Wang, ACS Nano 7 (2013) 9461–9468.
[36] Z. Zhao, X. Pu, C. Du, L. Li, C. Jiang, W. Hu, Z.L. Wang, ACS Nano 10 (2016) 1780–1787.
[37] A. Ahmed, I. Hassan, M. Hedaya, T.A. El-Yazid, J. Zu, Z.L. Wang, Nano Energy 36 (2017) 21–29.
[38] J. Chen, G. Zhu, W. Yang, Q. Jing, P. Bai, Y. Yang, T.C. Hou, Z.L. Wang, Adv. Mater. 25 (2013) 6094–6099.
[39] H. Zhang, Y. Yang, Y. Su, J. Chen, K. Adams, S. Lee, C. Hu, Z.L. Wang, Adv. Funct. Mater. 24 (2014) 1401–1407.
[40] Y. Zi, H. Guo, Z. Wen, M.H. Yeh, C. Hu, Z.L. Wang, ACS Nano 10 (2016) 4797–4805.
[41] Y. Xie, S. Wang, S. Niu, L. Lin, Q. Jing, J. Yang, Z. Wu, Z.L. Wang, Adv. Mater. 26 (2014) 6599–6607.
[42] A. Yu, M. Song, Y. Zhang, Y. Zhang, L. Chen, J. Zhai, Z.L. Wang, Nano Res. 8 (2015) 765–773.
[43] Q. Shi, T. He, C. Lee, Nano Energy 57 (2019) 851–871.
[44] C.B. Han, C. Zhang, X.H. Li, L. Zhang, T. Zhou, W. Hu, Z.L. Wang, Nano Energy 9 (2018) 325–333.
[45] Y. Chen, Y.C. Wang, Y. Zhang, H. Zou, Z. Lin, G. Zhang, C. Zou, Z.L. Wang, Adv. Energy Mater. 8 (2018) 1802159.
[46] H. Yang, W. Liu, Y. Xi, M. Lai, H. Guo, G. Liu, M. Wang, T. Li, X. Ji, X. Li, Nano Energy 47 (2018) 539–546.
[47] Z. Wen, Q. Shen, X. Sun, , Nano-Micro Lett. 9 (2017) 45.
[48] Y. Su, G. Xie, S. Wang, H. Tai, Q. Zhang, H. Du, H. Zhang, X. Du, Y. Jiang, Sens. Actuator B-Chem. 251 (2017) 144–152.
[49] H. Wang, H. Wu, D. Hasan, T. He, Q. Shi, C. Lee, ACS Nano 11 (2017) 10337–10346.
[50] Y. Su, G. Xie, H. Tai, S. Li, B. Yang, S. Wang, Q. Zhang, H. Du, H. Zhang, X. Du, Y. Jiang, Nano Energy 47 (2018) 316–324.
[51] C.H. Chen, P.W. Lee, Y.H. Tsao, Z.H. Lin, Nano Energy 42 (2017) 241–248.
[52] Z.H. Lin, G. Zhu, Y.S. Zhou, Y. Yang, P. Bai, J. Chen, Z.L. Wang, Angew. Chem. -Int. Ed. 52 (2013) 5065–5069.
[53] J. Tian, H. Feng, L. Yan, M. Yu, H. Ouyang, H. Li, W. Jiang, Y. Jin, G. Zhu, Z. Li, Z.L. Wang, Nano Energy 36 (2017) 241–249.
[54] Z. Liu, Y. Ma, H. Ouyang, B. Shi, N. Li, D. Jiang, F. Xie, D. Qu, Y. Zou, Y. Huang, H. Li, C. Zhao, P. Tan, M. Yu, Y. Fan, H. Zhang, Z.L. Wang, Z. Li, Adv. Funct. Mater. (2018) 1807560.
[55] D. Choi, Y.H. Tsao, C.M. Chiu, D. Yoo, Z.H. Li, D.S. Kim, Nano Energy 38 (2017) 419–427.
[56] T.H. Chang, Y.W. Peng, C.H. Chen, T.W. Chang, J.M. Wu, J.C. Hwang, J.Y. Gan, Z.H. Lin, Nano Energy 21 (2016) 238–246.
[57] S. Wang, G. Xie, H. Tai, Y. Su, B. Yang, Q. Zhang, X. Du, Y. Jiang, Nano Energy 51 (2018) 231–240.
[58] C.B. Han, T. Jiang, C. Zhang, X. Li, C. Zhang, X. Cao, Z.L. Wang, ACS Nano 9 (2015) 12552–12561.
[59] Y. Tang, Z. Li, J. Ma, L. Wang, J. Yang, B. Du, Q. Yu, X. Zu, Sens. Actuator B-Chem. 215 (2015) 283–291.
[60] X. Qiu, R. Tang, J. Zhu, J. Oiler, C. Yu, Z. Wang, H. Yu, Sens. Actuator B-Chem. 147 (2010) 381–384.
[61] X. Wang, B. Ding, J. Yu, M. Wang, F. Pan, Nanotechnology 21 (2009) 055502.
[62] X. Le, F. Ma, D. Li, J. Pang, Z. Xu, C. Gao, J. Xie IEEE Micro Electro Mechanical Systems (MEMS), Belfast, North Ireland, 2018, pp. 928–931.
[63] H.J. Lee, K.K. Park, M. Kupnik, N.A. Melosh, B.T. Khuri-Yakub, Anal. Chem. 84 (2012) 3063–3066.
[64] S. Borini, R. White, D. Wei, M. Astley, S. Haque, E. Spigone, N. Harris, J. Kivioja, T. Ryhanen, ACS Nano 7 (2013) 11166–11173.
[65] Z.B. Aziza, K. Zhang, D. Baillargeat, Q. Zhang, Appl. Phys. Lett. 107 (2015) 134102.
[66] K. Narimani, F.D. Nayeri, M. Kolahdouz, P. Ebrahimi, Sens. Actuator B-Chem. 224 (2016) 338–343.
[67] D. Zhang, Y. Sun, P. Li, Y. Zhang, ACS Appl. Mater. Interfaces 8 (2016) 14142–14149.
[68] H. Guo, J. Chen, L. Tian, Q. Leng, Y. Xi, C. Hu, ACS Appl. Mater. Interfaces 6 (2014) 17184–17189.
[69] S. Fanget, S. Hentz, P. Puget, J. Arcamone, M. Matheron, E. Colinet, P. Andreucci, L. Duraffourg, E. Myers, M.L. Roukes, Sens. Actuator B-Chem. 160 (2011) 804–821.
[70] J. Shah, R. Kotnala, B. Singh, H. Kishan, Sens. Actuator B-Chem. 128 (2007) 306–311.
[71] Q. Lin, Y. Li, M. Yang, Sens. Actuator B-Chem. 161 (2012) 967–972.
[72] Z. Yuan, H. Tai, Z. Ye, C. Liu, G. Xie, X. Du, Y. Jiang, Sens. Actuator B-Chem. 234 (2016) 145–154.
[73] D. Zhang, D. Wang, X. Zong, G. Dong, Y. Zhang, Sens. Actuator B-Chem. 262 (2018) 531–541.
[74] X. Leng, D. Luo, Z. Xu, F. Wang, Sens. Actuator B-Chem. 257 (2018) 372–381.
[75] J. Paredes, S. Villar-Rodil, A. Martínez-Alonso, J. Tascon, Langmuir 24 (2008) 10560–10564.
[76] Y. Yao, X. Chen, H. Guo, Z. Wu, Appl. Surf. Sci. 257 (2011) 7778–7782.
[77] X. Le, X. Wang, J. Pang, Y. Liu, B. Fang, Z. Xu, C. Gao, Y. Xu, J. Xie, Sens. Actuator B-Chem. 255 (2018) 2454–2461.
[78] X. Li, X. Chen, Y. Yao, N. Li, X. Chen, X. Bi, IEEE Sens. J. 13 (2013) 4749–4756.
[79] H.W. Yu, H.K. Kim, T. Kim, K.M. Bae, S.M. Seo, J.M. Kim, T.J. Kang, Y.H. Kim, ACS Appl. Mater. Interfaces 6 (2014) 8320–8326.
[80] D. Zhang, D. Wang, P. Li, X. Zhou, X. Zong, G. Dong, Sens. Actuator B-Chem. 255 (2018) 1869–1877.
[81] E. Singh, M. Meyyappan, H.S. Nalwa, ACS Appl. Mater. Interfaces 9 (2017) 34544–34586.
[82] G. Zhou, J.H. Byun, Y. Oh, B.M. Jung, H.J. Cha, D.G. Seong, T.W. Chou, ACS Appl. Mater. Interfaces 9 (5) (2017) 4788–4797.
[83] T. Yamashita, S. Takamatsu, H. Okada, T. Itoh, T. Kobayashi, IEEE Sens. J. 16 (2015) 8840–8846.
[84] A.I. Uddin, P.S. Kumar, K. Hassan, H.C. Kim, Sens. Actuator B-Chem. 258 (2018) 857–869.
[85] Z.H. Lin, G. Cheng, W. Wu, K.C. Pradel, Z.L. Wang, ACS Nano 8 (2014) 6440–6448.
[86] H. Zhu, N. Wang, Y. Xu, S. Chen, M. Willander, X. Cao, Z.L. Wang, Adv. Funct. Mater. 26 (2016) 3029–3035.
[87] H. Tai, Y. Zhen, C. Liu, Z. Ye, G. Xie, X. Du, Y. Jiang, Sens. Actuator B-Chem. 230 (2016) 501–509.
[88] Z.Y. Sui, Y. Cui, J.H. Zhu, B.H. Han, ACS Appl. Mater. Interfaces 5 (2013) 9172–9179.
[89] C. Sun, S. Jiang, Y. Liu, Sensors 18 (2018) 703.

[90] H.J. Lee, K.K. Park, M. Kupnik, B.T. Khuri-Yakub, Sens. Actuator B-Chem. 174 (2012) 87–93.
[91] S. Cui, Y. Zheng, T. Zhang, D. Wang, F. Zhou, W. Liu, Nano Energy 49 (2018) 31–39.
[92] D. Hasan, C. Lee, Adv. Sci. 5 (2018) 1700581.
[93] W. Xuan, M. Cole, J.W. Gardner, S. Thomas, F.H. Villa-López, X. Wang, S. Dong, J. Luo, J. Micromech. Microeng. 27 (2017) 055017.
[94] S. Mali, L.S. Sakanaka, F. Yamashita, M. Grossmann, Carbohydr. Polym. 60 (2005) 283–289.
[95] A.J. Nolte, N.D. Treat, R.E. Cohen, M.F. Rubner, Macromolecules 41 (2008) 5793–5798.
[96] H. Zhang, Y. Yang, Y. Su, J. Chen, C. Hu, Z. Wu, Y. Liu, C.P. Wong, Y. Bando, Z.L. Wang, Nano Energy 2 (2013) 693–701.

Changhe Sun received the B.Eng. degree from College of Optoelectronic Engineering at Chongqing University, China, in 2014. He is currently pursuing his Ph.D. in Instrument Science and Technology with Chongqing University, China. From 2017 to 2018, he was a visiting Ph.D. student in the Department of Electrical and Computer Engineering at National University of Singapore. His research interests focus mainly on piezoelectric/capacitive ultrasonic transducers, MEMS based resonant sensors and their applications.

Qiongfeng Shi received his B.Eng. degree from the Department of Electronic Engineering and Information Science, University of Science and Technology of China (USTC) in 2012, and received his Ph.D. degree from the Department of Electrical and Computer Engineering, National University of Singapore (NUS) in 2018. He is currently a Research Fellow in the Department of Electrical and Computer Engineering, National University of Singapore. His research interests include energy harvesters, triboelectric nanogenerators, self-powered sensors, and wearable/implantable electronics.

Dihan Hasan received his B.Eng. degree from Department of Electrical and Electronic Engineering at Bangladesh University of Engineering and Technology in 2012 and Ph.D. degree from Department of Electrical and Computer Engineering at National University of Singapore in 2018. He is currently a Research Fellow of Electrical and Computer Engineering at National University of Singapore. His research interests include plasmonics, Si photonics and energy harvesting.

Mahmut Sami Yazici received his B.S. degree in Electrical and Electronics Engineering and B.S. degree in Physics from Bogazici University, Istanbul/Turkey, in 2017. Currently, he is pursuing his Ph.D. in the Electrical and Computer Engineering Department at NUS. His main research focus is MEMS based IR sensors.

Minglu Zhu received his B.Bus. degree in Business Administration from the School of Business at State University of Bangladesh, Dhaka, Bangladesh, in 2010, and B.Sc. degree in Materials Science and Engineering from the School of Materials Science and Engineering at University of Illinois at Urbana-Champaign, Illinois, United States, in 2014. He is now a Ph.D. student at the Department of Electrical & Computer Engineering, NUS. His research interests focus mainly on MEMS based energy harvesters and self-powered sensors.

Yiming Ma received his B.Eng. degree in Mechatronics Engineering from the School of Mechanical Engineering at Zhejiang University, Hangzhou, China, in 2016. Currently, he is a Ph.D. student in the Department of Electrical & Computer Engineering at National University of Singapore. His research interests focus mainly on integration of MEMS with nanophotonics.

Bowei Dong received his B.S degree in Physics and Mathematics from the School of Physical and Mathematical Sciences of Nanyang Technological University in 2015 with the support from 'Senior Middle II Scholarship' awarded by the Ministry of Education, Singapore. Starting from 2015, he became a Ph.D. student in NUS Graduate School for Integrative Sciences and Engineering with the support from 'A*STAR Graduate Scholarship' awarded by A*STAR Singapore. His research interest includes mid-IR photonics for healthcare and environmental monitoring applications. He is also interested in self-powered wearable photonics devices.

Yufei Liu received B.S. degree in Physics and B.A. in Economics in 2003 from Peking University, the M.Eng. degree in Microelectronics and Solid State Electronics in 2006 from the Shanghai Institute of Microsystem and Information Technology, Chinese Academy of Science, and Ph.D. degree in 2011 from Heriot-Watt University. He is currently a Professor and Director of the Centre for Intelligent Sensing Technology, College of Optoelectronic Engineering, Chongqing University and his research interests are advance micro/nano fabrication, micro-electro-mechanical system (MEMS) technology, and multi-functional microsystem for precision biomedical application.

Chengkuo Lee received his Ph.D. degree in Precision engineering from The University of Tokyo in 1996. Currently, he is the director of Center for Intelligent Sensors and MEMS, and an Associate Professor in the Department of Electrical and Computer Engineering, National University of Singapore, Singapore. In 2001, he cofounded Asia Pacific Microsystems, Inc., where he was the Vice President. From 2006 to 2009, he was a Senior Member of the Technical Staff at the Institute of Microelectronics, A-STAR, Singapore. He has contributed to more than 300 international conference papers and extended abstracts and 270 peer-reviewed international journal articles.